Microphase Separation in Model 4-Miktoarm Star Copolymers of the AB3Type

ARTICLE *in* MACROMOLECULES · MAY 1997

Impact Factor: 5.8 · DOI: 10.1021/ma961624l

4 AUTHORS, INCLUDING:

George Floudas
University of Ioannina
229 PUBLICATIONS **4,182** CITATIONS
SEE PROFILE

Igor Erukhimovich
Lomonosov Moscow State University
100 PUBLICATIONS **1,445** CITATIONS
SEE PROFILE

Microphase Separation in Model 4-Miktoarm Star Copolymers of the AB_3 Type

G. Floudas*

Foundation for Research and Technology-Hellas (FORTH), Institute of Electronic Structure and Laser, P.O. Box 1527, 711 10 Heraklion, Crete, Greece

N. Hadjichristidis and Y. Tselikas

Department of Chemistry, University of Athens, Panepistimiopolis, Zografou 15771, Athens, Greece, and FORTH, P.O. Box 1527, 711 10 Heraklion, Crete, Greece

I. Erukhimovich

Department of Physics, Moscow State University, Moscow 117234, Russia

Received November 4, 1996; Revised Manuscript Received January 24, 1997[⊗]

ABSTRACT: The order−disorder transition has been studied in two AB_3 miktoarm stars of styrene and isoprene with SAXS and rheology. A mean-field theory has been developed to treat the most general case of miktoarm stars: A_mB_n ($m \neq n$) which provides the phase stability criteria and the static structure factor in the disordered phase. The theory predicts a maximum in the critical value of χN_t ($N_t = N_A + nN_B$) as a function of the number of arms n in AB_n, for $n = 3$. This maximum arises from a delicate balance between the stretching free energies of the A and B blocks forming the miktoarm stars. The theoretical predictions for the phase stability and the structure factor have been tested experimentally, using SAXS, and the interaction parameter has been extracted. The latter exhibits a weak T-dependence which is consistent with fluctuation effects near the transition. Further evidences for the existence of fluctuations at temperatures above and below the transition are provided by (i) the nonlinearity of the inverse peak intensity vs inverse temperature, in the disordered state, and (ii) the existence of metastable states in the ordered state. All SAXS peak parameters were discontinuous at the order-to-disorder transition, revealing a first-order transition.

Introduction

It is well-known that block copolymer additives can effectively compatibilize immiscible polymer blends.[1] These molecules act as surfactants: they localize at interfaces, lower the interfacial tension and reduce the phase size of the otherwise macrophase separated system. The relation between macromolecular architecture and compatibilizer efficiency has only recently started to be explored.[2] Nonlinear block copolymers, such as graft copolymers, have had very little attention despite of their great commercial importance. Only recently, model graft and miktoarm (from the Greek word *μικτός* meaning mixed) star copolymers of the A_mB_n type have been synthesized with specific arm numbers, composition, and molecular weight and with a narrow distribution of molecular weight by anionic polymerization techniques.[3−5] These systems opened new directions both for experiment[5−7] and theory,[8] mainly because of their intrinsic compatibility, which depends on the number of arms and therefore can be controlled at the synthetic level. Here we define the intrinsic compatibility by the critical value of the product χN_t, where χ is the interaction parameter, N_t is the total degree of polymerization ($=N_A + nN_B$, and N_A, N_B are the degrees of polymerization of the A and B blocks, respectively, in the AB_n miktoarm star) and $(\chi N_t)_c$ is the critical value of χN_t for the stability of the disordered phase. In the simplest approximation, χ is inversely proportional to T, and $(\chi N_t)_c$ being higher for miktoarm stars than for linear diblock copolymers simply means that the T-range of the homogeneous phase is significantly enlarged in the former systems.

The potential of miktoarm stars, apart from their intrinsic compatibility, is that they allow for a coherent investigation of the influence of macromolecular architecture on (i) the static structure factor, (ii) the thermodynamics of the process of microphase separation (e.g. order of the transition), (iii) the extent of the fluctuation-controlled regime, (iv) the self-assembling mechanism, and, finally, (v) the dynamics of chains confined in microstructures with additional topological constraints. Here we will consider (i)−(iv) using a specific example of a miktoarm star.

The phase stability criteria and the structure factor in the disordered phase have been calculated in the context of the mean-field theory (MFT) first for linear diblocks[9] and triblocks[10−13] and subsequently for graft[11,14,15] and star[11,15] block copolymers. However, a generalization of the theory to A_mB_n miktoarm stars was still missing as well as experiments which can probe the static structure factor. In the present study the MFT predictions for the structure factor are extended to include the most general case of miktoarm stars, namely, A_mB_n with $m \neq n$. Furthermore, the effect of varying the number of B-blocks on the spinodal curves of AB_n's has been examined. These theoretical predictions for the structure factor in the homogeneous phase and for the phase stability have been tested experimentally using SAXS, for what proves to be the most interesting case of a miktoarm star of the AB_n type, namely the system AB_3. Moreover, we have employed rheology and SAXS and identified the order-to-disorder transition (ODT) by observing discontinuous changes in the peak parameters and shear moduli, respectively. Using the same techniques we account for fluctuation effects above and below the ODT, respectively, from the nonlinearity of the inverse peak intensity vs inverse temperature and the existence of metastable states.

[⊗] Abstract published in *Advance ACS Abstracts,* May 1, 1997.

S0024-9297(96)01624-5 CCC: $14.00

Table 1. Molecular Characteristics of the AB_3 Miktoarm Stars

sample	$\bar{M}_n$(PS)[a] × 10^3	$\bar{M}_n{}^{arm}$(PI)[a] × 10^3	$\bar{M}_n{}^{total}$ × 10^3	$\bar{M}_w/\bar{M}_n$[b]	wt % PS[c]	$N_n{}^{total}$	f_{PS}[d]	T_{ODT} (K)
SI_3-40	35.2	14.5	77.2	1.05	41	946	0.40	370
SI_3-45	35.2	12.4	73	1.05	50	865	0.45	361

[a] Membrane osmometry in toluene at 34 °C. [b] By LALLS in THF at 25 °C. [c] By SEC in THF at 30 °C. [d] Calculated from $N_n = N^*_{n,PS} + N^*_{n,PI} = N_{n,PS}(\rho^*_I/\rho^*_S)^{1/2} + N_{n,PI}(\rho^*_S/\rho^*_I)^{1/2}$, and $f = N^*_{n,PS}/N_n$ where $N_{n,i}$ are the degrees of polymerization for each block and ρ^*_i are the molar densities.

This fluctuation-controlled regime in the AB_3 miktoarms is found to be enlarged as compared with linear block copolymers.

Experimental Section

Samples. The molecular characteristics of the two AB_3 miktoarm stars are given in Table 1. The morphology of the same samples have been studied earlier[7] by SAXS and TEM in the undiluted state and revealed the formation of PS cylinders with hexagonal symmetry. However, both copolymers are strongly segregated, and a study of the order-to-disorder transition in the melt state is not possible. Here we added the neutral solvent dioctyl phthalate (DOP) ($\varphi_p = 0.42$) to reduce the T_{ODT} to the experimentally accessible temperature range.

Small-Angle X-ray Scattering. The SAXS measurements were performed with a Kratky compact camera (Anton Paar KG) equipped with a one-dimensional position sensitive detector (M. Braun). The Ni-filtered Cu Kα radiation ($\lambda = 0.154$ nm) was used from a Siemens generator operating at 35 kV and 30 mA. The samples were inserted in a special furnace and all measurements were made under vacuum. Measurements of 1 h long were made at intervals of 5 K within the range 298−423 K with a stability better than ±0.2 K. Between successive temperatures, a 30 min waiting time was preset for equilibration. The data were collected in a multichannel analyzer and transferred to a Vax station for further analysis. The data were corrected for absorption, background scattering, and slit-length smearing.[16] Intensities in absolute units were determined by using the moving slit method.

Rheology. The storage and loss moduli G' and G'' have been measured using a Rheometric Scientific dynamic stress rheometer (DSR) with a controlled strain option. The oscillatory mode with a parallel-plate sample geometry was used. The gap was set to 0.5 mm, and the sample temperature was controlled by two electrically heated plates within the range 300−400 K with a stability better than 0.1 K. Typically four experiments have been performed: First, the linear and nonlinear viscoelastic ranges have been identified by studying the strain dependence of the complex shear modulus G^* ($=(G'^2 + G''^2)^{1/2}$). For the remaining experiments, low deformations were used which where well within the linear viscoelastic range. Second, isothermal frequency scans were made at $\omega = 1$ rad/s aiming to identify the T_{ODT}. Third, isothermal frequency scans have been performed at temperatures below and above the ODT within the frequency range $10^{-2} < \omega < 10^2$ rad/s. Last, isothermal/isochronal scans at $\omega = 1$ rad/s, were made for two samples following a quench from the disordered phase to different final temperatures within the ordered phase.

Results and Discussion

Disordered Phase and Order-to-Disorder Transition. Some typical SAXS spectra for the SI_3-45 miktoarm diluted with DOP are shown in Figure 1, in the vicinity of the order-to-disorder transition. The latter is identified by the discontinuous drop of the peak intensity at approximately 361 K. At temperatures below the T_{ODT}, additional reflections appear at higher Q values, at positions $3^{1/2}$ and $4^{1/2}$ relative to the main peak at Q^* (inset to Figure 1), which are suggestive of a hexagonal arrangement of PS cylinders. A hexagonal lattice formed by the PS cylinders was the morphology in the undiluted miktoarms as shown by TEM and SAXS.[7] The main peak parameters are plotted in

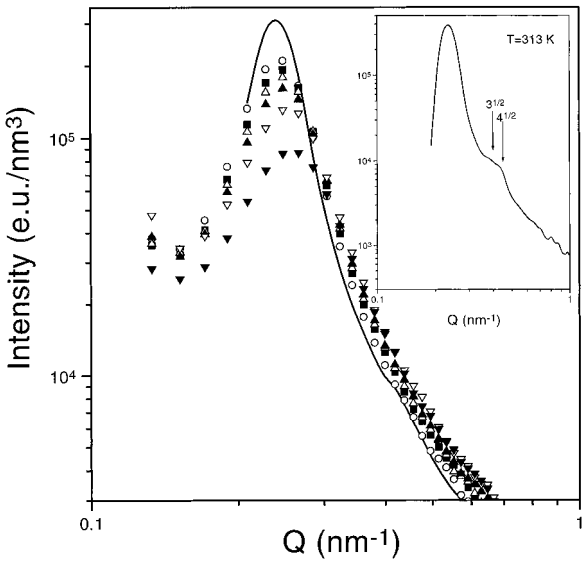

Figure 1. SAXS intensity profiles for the SI_3-45 miktoarm copolymer diluted with DOP ($\varphi_P = 0.42$) in the vicinity of the order-to-disorder transition ($T_{ODT} \approx 361$ K). Only data at some selected temperatures (K) are shown: (—) 358; (○) 363; (■) 374; (△) 380; (▲) 388; (▽) 403; (▼) 423.

Figure 2 as a function of inverse temperature. In all cases, the peak parameters were extracted using a Lorentzian fitting function both below and above T_{ODT}. All parameters are discontinuous at the ODT (shown by the vertical line). Such discontinuities are important since they reveal a first-order transition. It is worth noticing that for asymmetric block copolymers both the MFT[9] and the fluctuation approach by Fredrickson and Helfand[17] predict a first-order transition. However, the inverse peak intensity varies nonlinearly with inverse temperature above the T_{ODT}. The nonlinearity of $I(Q^*)^{-1}$ vs T^{-1} violates the MFT predictions but is predicted by the fluctuation approach.[17] Notice that the T-range of curvature is much too broad as compared to those for undiluted copolymers, which may suggest a broader range of temperatures where the fluctuation effects dominate. The peak position at Q^* has also a pronounced T-dependence both below and above the T_{ODT} and is discontinuous in the vicinity of the transition. A discontinuous change of Q^* toward smaller values with increasing T has also been reported in asymmetric linear diblocks,[6] in asymmetric graft copolymers of the AB_2 type,[18] and, to a lesser extent, in diblock copolymer/homopolymer blends.[19] The $Q^*(T)$ in Figure 2 displays a stronger T-dependence above the ODT ($Q^*(T > T_{ODT}) = 0.359 - 42/T$ as compared to $Q^*(T < T_{ODT}) = 0.31 - 23/T$). In the framework of the MFT, Q^* should be independent of temperature.

In the context of the mean-field theory the structure factor for the concentration fluctuations in undiluted homogeneous block copolymers is given by the general expression[9−11]

$$\frac{N}{S(Q)} = \tilde{g}(x,f) - 2\tilde{\chi} \qquad (1)$$

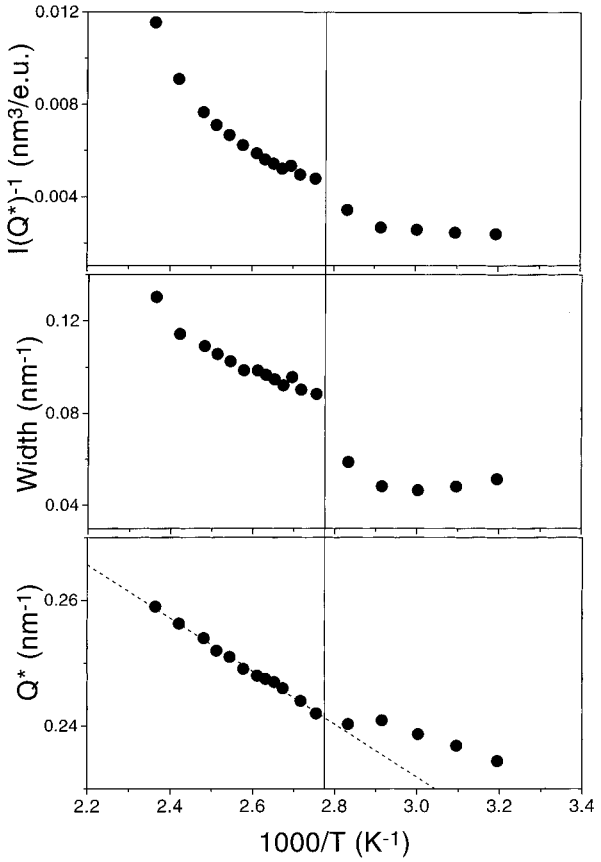

Figure 2. Inverse peak intensity, peak width and peak position plotted vs inverse temperature for the SI_3-45/DOP miktoarm copolymer. The vertical line signifies the T_{ODT}.

with

$$\tilde{g}(x,f) = \frac{g_{AA}(x,f)g_{BB}(x,f) - g_{AB}^2(x,f)}{g_{AA}(x,f) + g_{BB}(x,f) + g_{AB}(x,f) + g_{BA}(x,f)} \quad (2)$$

where the components $g_{i,j}$ of the structural matrix **g**, for the general case of miktoarms A_m B_n, are given by

$$g_{AA} = mg_D(x,f) + m(m-1)[F(x,f)]^2 \quad (3)$$

$$g_{BB} = ng_D(x,1-f) + n(n-1)[F(x,1-f)]^2 \quad (4)$$

$$g_{AB} = g_{BA} = mnF(x,f)F(x,1-f) \quad (5)$$

and $\tilde{\chi} = \chi N/[mf + n(1-f)]$ with $x = Q^2a^2N/6$

$$g_D(x,f) = \frac{2}{x^2}[e^{-xf} - 1 + xf] \quad (6)$$

and

$$F(x,f) = \frac{1 - e^{-xf}}{x} \quad (7)$$

In the above equations we are using the block parameters N ($=N_A + N_B$) and f ($=N_A/N$)—which are different from the AB_n star parameters N_t ($=N_A + nN_B$) and f_A ($=N_A/N_t$) to appear later. For the miktoarm stars studied here, $m = 1$ and $n = 3$, and the expressions above are considerably simplified.

Using these expressions, the spinodal curves have been calculated for the series of AB_n miktoarm stars, and the results for the lower members of the series are plotted in Figure 3a. In general, graft copolymers are more difficult to phase separate than linear diblocks and this is reflected in the value of χN_t being higher than the diblock case at any f_A. Moreover, the spinodal curves become asymmetric due to the inherent asymmetry of miktoarm stars. There are some interesting trends found within the class of the miktoarm copolymers, by increasing n. For n up to 3 there is a considerable increase in the critical value of χN_t—which indicates an increasing compatibility between the A and B blocks. However, for $n > 3$, there is a reversal in $(\chi N_t)_c$ as shown in Figure 3b, which starts to decrease and for $n > 10$, differs only slightly from that of the AB diblock copolymer. The crossing of the spinodal curves for AB_3 and AB_4 creates an interesting situation: there is a decrease in T_{ODT} for $f_A = 0.3$ in going from AB_3 to AB_4 but an increase for the antisymmetric composition ($f_A = 0.7$). In the Figure 3a, we have included the existing experimental χN_t values from an AB_2 miktoarm star and the two AB_3 employed here, indicating the investigated χN_t range (see below).

In order to understand the behavior of the spinodal curves shown in Figure 3 in a crude but qualitatively reasonable way, let us represent the quadratic contribution to the conformational free energy as the sum of the corresponding contributions for the system of so-called broken blocks[10] as

$$\Delta F_{conf} = \Delta F_{conf}^{A} + \Delta F_{conf}^{B} \quad (8)$$

where $\Delta F_{conf}^{i} \sim g_{ii}^{-1}(x^*,f)\,\delta\phi_i^2(x^*)$, $g_{ii}(x^*,f)$ is the structure factor for the system of broken blocks of type i (i = A or B), and $x^* = (Q^*R_{g,i})^2$ is the value of x at the critical wavelength calculated for miktoarm stars. In other words, we consider both partial contributions of the broken blocks as functions of the period L (or the corresponding wavenumber $Q = 2\pi/L$) of the density waves arising in the system. From eqs 6 and 8, it follows that ΔF_{conf}^{i} is an increasing function of the ratio R_G^i/L. Therefore, this ratio can be considered as a measure of the contribution to the total conformational free energy due to the stretching of broken blocks which is caused by the spatially periodic external field (ordered system).

The ratios R_G^i/L for the system AB_n with $n = 1$, 2, 3, and 4 are plotted in parts a and b of Figure 4 for the A- and B-blocks, respectively. At a given value of n the ratio R_G^A/L increases monotonously with increasing f_A. The situation for the B-blocks (Figure 4b), however, is just the opposite: R_G^B/L decreases both with increasing f_A and n, and therefore the stretching free energy decreases. The competition in the stretching free energies of the A- and B-blocks results in the maximum $(\chi N_t)_c$ at a finite value of n. Further insight can be gained by considering that the blend is now composed of an A-block and a B-star instead of broken B-blocks. The result for the ratio R_G^{B-star}/L is plotted in Figure 4c as a function of f_A for $n = 1$, 2, 3, and 4. Although the ratios are decreasing functions of composition f_A, their dependence on n is more complicated: for AB_2 this ratio is higher than for AB at all compositions but for AB_3 this holds only for compositions lower than the critical one ($f < f_c$) whereas for $f > f_c$ the ratio is smaller in the miktoarm stars than in the diblock copolymer. Therefore, the expectation is that the tendency for a decrease in the stretching free energy of the B-stars wins for comparatively large values of f_A. This qualitative conclusion is in accord with the variation of the optimal composition $f_A(n)$ (corresponding to the minima of the $\chi N_t(f_A)$ curves, Figure 3b) obtained via the exact calculation (eq 2).

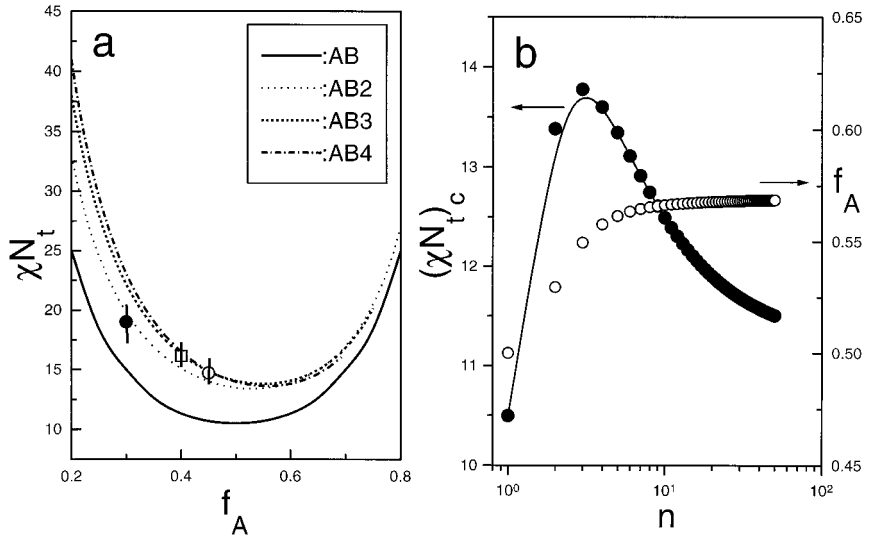

Figure 3. (a) Comparison of the spinodal curves $\chi N_t(f_A)$ for diblock and different AB_n miktoarm copolymers with $n = 2$, 3, and 4. The experimental results from an AB_2 (●) and the two AB_3 (□, ○) miktoarm stars are shown together with the investigated temperature range (vertical lines). (b) Critical values of χN_t plotted as a function of the number of arms of the B-blocks. The dependence of the optimal composition corresponding to the minima of the spinodal curves is also shown. The line is only a quide to the eye.

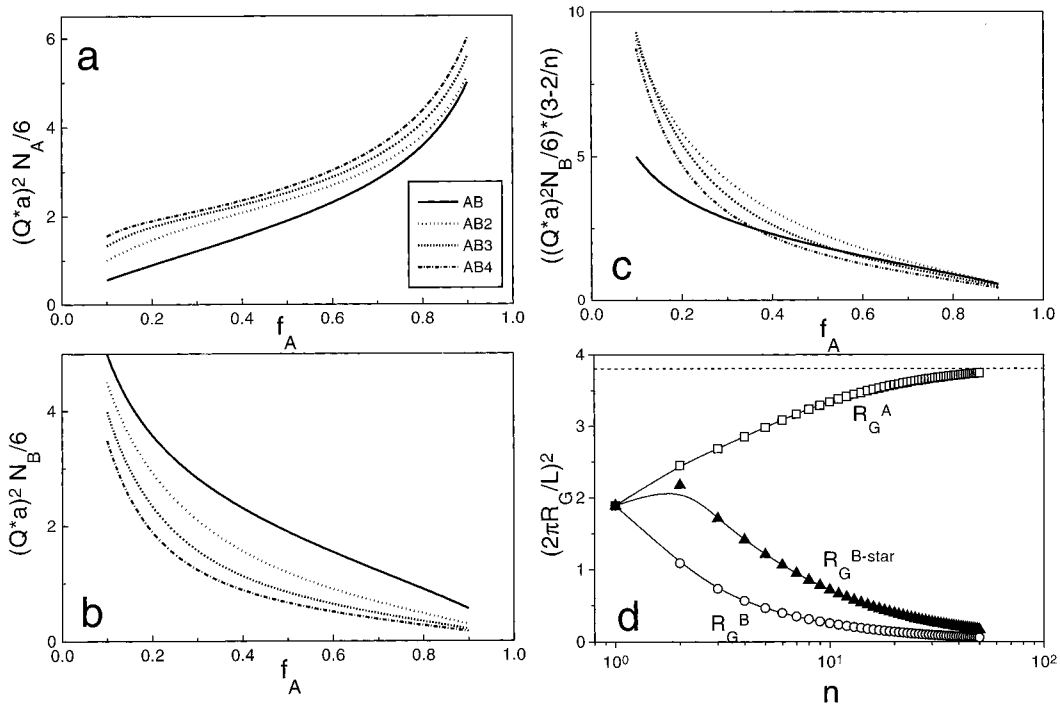

Figure 4. R_G^i/L, calculated for the system of broken blocks comprising the miktoarm AB_n, with $n = 1$, 2, 3, and 4, shown separately for (a) the A-block, (b) the B-blocks and (c) the B-stars as a function of composition f_A. (d) The same ratio plotted as a function of n at the optimal values of composition f_A. Solid lines are splines through the data. The dashed line correspond to the the pure diblock case.

Some complementary information can be extracted by plotting the ratio R_G/L, for compositions corresponding to the minima of Figure 3a, as a function of the number of B-arms. The results for the blends composed of A- and broken B-blocks as well as for A- and B-stars are shown in Figure 4d. This ratio, and the corresponding stretching free energy, increases for the A-block and decreases for the broken B-blocks whereas for the B-stars it goes through a maximum at $n \approx 2$. Notice, that the limiting value for the A-block (shown with a dashed line in the figure) corresponds to ~3.8, which is the value for a symmetric diblock copolymer. In summary, the maximum in $(\chi N_t)_c(f_A)$ at $n \approx 3$ results from a delicate balance between the stretching free energies of the A- and B-blocks whereas for $n \gg 3$ the free energy of the system is mainly determined by the B-blocks forming the star.

The predictions of the MFT for the structure factor have been tested for linear[20−24] and recently for nonlinear[25,6,18] block copolymers and found to fit qualitatively the experimental profiles only for $T \gg T_{ODT}$. For diblock copolymer solutions, however, the above formalism can only be applied under the following conditions:[26] (i) the solvent is equally good for both blocks (i.e., $\chi_{SD} \approx \chi_{ID}$, where χ_{AD} is the segmental interaction parameter between the A-block and the solvent) and (ii) the optical θ-condition is satisfied: $n^{ex}{}_{PS} f_{PS} + n^{ex}{}_{PI}(1 - f_{PI}) = 0$, where $n^{ex}{}_i$ are the excess electron densities of PS and

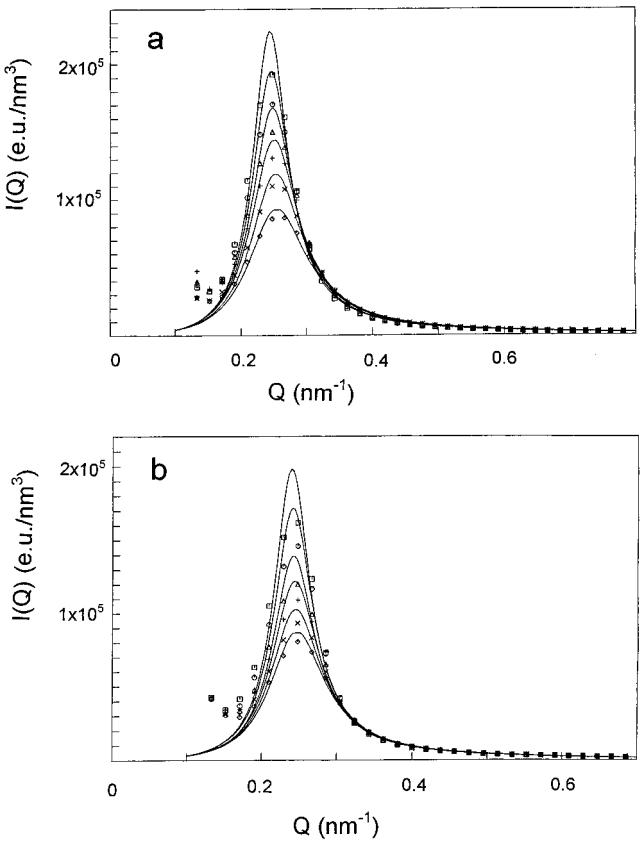

Figure 5. SAXS profiles for SI_3-45/DOP (top) and SI_3-40/DOP (bottom) fitted to the MFT at different temperatures as indicated: (a) (□) 423, (○) 413, (△) 403, (+) 393, (×) 383, and (◇) 374 K; (b) (□) 423, (○) 413, (△) 403, (+) 393, (×) 383, and (◇) 373 K.

PI blocks relative to that of DOP. Under these conditions the SAXS intensity for the SI/DOP solutions can be written as

$$I(Q) = (n_{PS} - n_{PI})^2 VS(Q) \qquad (9)$$

where the first term is the electron density difference between the two blocks and the interaction term in $S(Q)$ is modified to an effective interaction parameter $\chi_{eff} = \chi_o \varphi_P$, where χ_o is the bare interaction parameter between styrene and isoprene and φ_P is the polymer concentration.[27]

The fits of the SAXS profiles to the MFT are shown in Figure 5 for the SI_3-45 and SI_3-40 miktoarm stars diluted with DOP, for temperatures in the range $373 < T < 423$ K. Systematic deviations exist up to the highest measurement temperature, i.e., at $T_{ODT} + 62$ K for the former and to $T_{ODT} + 53$ K for the latter. The cause of such deviations can be either the failure of the optical θ-condition and/or an increase of the fluctuation controlled regime. However, given the higher curvature in the intensity data of Figure 2, the latter seems more plausible. For undiluted linear and nonlinear block copolymers the corresponding temperature range is much smaller (≤30 K). The temperature dependence of the effective interaction parameter $\chi_{eff}N_t$ extracted from the fits is plotted in Figure 6 as a function of inverse temperature. Similar to the inverse peak intensity (Figure 2), there is a curvature in the data followed by a levelling off as we approach the transition. We can use the highest temperature data to obtain a linear $\chi(T)$ dependence which can be parametrized as: $\chi_o = \chi_{eff}/\varphi_P = 0.03 + 4.4/T$ for SI_3-40 and $\chi_o = 0.02 + 6.3/T$ for SI_3-45. The calculation of χ_o is based on the

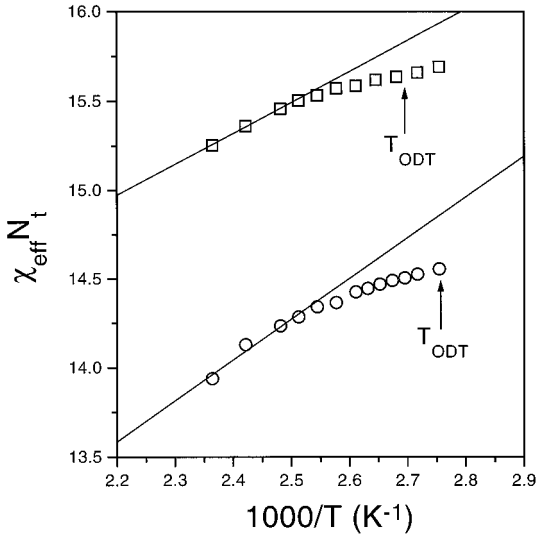

Figure 6. Temperature dependence of $\chi_{eff}N_t$ for the SI_3-40/DOP (□) and SI_3-45/DOP (○). The corresponding order-to-disorder transition temperatures are indicated with arrows.

statistical volume $(u_{PS}u_{PI})^{1/2}$ of 144 Å^3. Both dependencies are weaker than for the undiluted linear diblock copolymers when fitted to the MFT ($\chi_{SI} = 0.04 + 10/T$). Such an architecture-induced change of the bare interaction parameter has been reported earlier for star diblock copolymers of styrene and isoprene.[25,18] As expected, the experimental $\chi_{eff}N_t$ values are in agreement with the theoretical predictions (Figure 3a). In the same figure the χN_t from a (polystyrene)(polyisoprene)$_2$ miktoarm star[6] with $f_{PS} = 0.3$ is also included. These experimental results on the AB_2 and AB_3 miktoarm stars demonstrate the effect of increasing the number of B-blocks on the intrinsic compatibility, in agreement with theory.

Rheology is known to be a very sensitive technique for detecting the dissolution of the ordered structures formed in block copolymers.[6,18,19,28,29] Isochronal measurements of the storage modulus $G'(T)$, performed at low frequencies by heating the specimen provide the most accurate way of determining the T_{ODT}. The results of the isochronal measurements for the storage and loss moduli of the SI_3-45 and SI_3-40 miktoarms are shown in Figures 7 and 8, respectively. The abrupt change of G' at 361 and 370 K, signifies the order-to-disorder transition temperatures in agreement with the results from SAXS. Measurements with a higher temperature resolution performed at lower frequencies (inset to Figure 7) provide the T_{ODT} with an accuracy of better than 1 K. Isothermal frequency scans have also been performed at different temperatures below and above the transition and the results of the attempted time−temperature superposition (TTS) are shown in Figure 9 for the SI_3-45/DOP.

Strictly speaking, the principle of TTS is valid only for thermorheologically simple (homogeneous) polymer systems, and ordered block copolymers can not be considered as such. We are using this method here to compare the frequency dependencies above and below the ODT, but we use the isochronal measurements to identify the T_{ODT}. The shifted data in Figure 9 demonstrate the failure of the TTS at temperatures below the T_{ODT} and for frequencies smaller than some characteristic frequencies ω_1 and ω_2 for the G' and G'' data, respectively. Only for temperatures above the T_{ODT} does the principle of TTS work well, and the moduli exhibit typical terminal behavior with $G' \approx \omega^2$ and $G'' \approx \omega$. At lower temperatures the moduli exhibit weak frequency

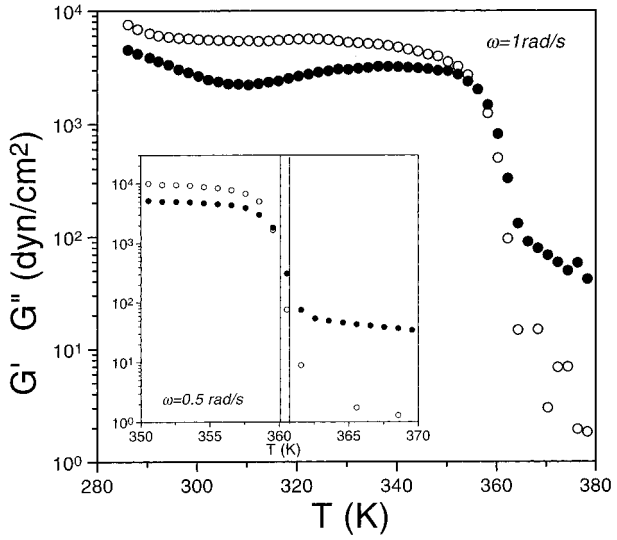

Figure 7. Isochronal measurements of the storage and loss moduli of the miktoarm SI_3-45/DOP measured at 1 rad/s with a heating rate of 2 K/min. The inset gives the result of an isochronal measurement ($\omega = 0.5$ rad/s) made with a slower heating rate (1 K/min).

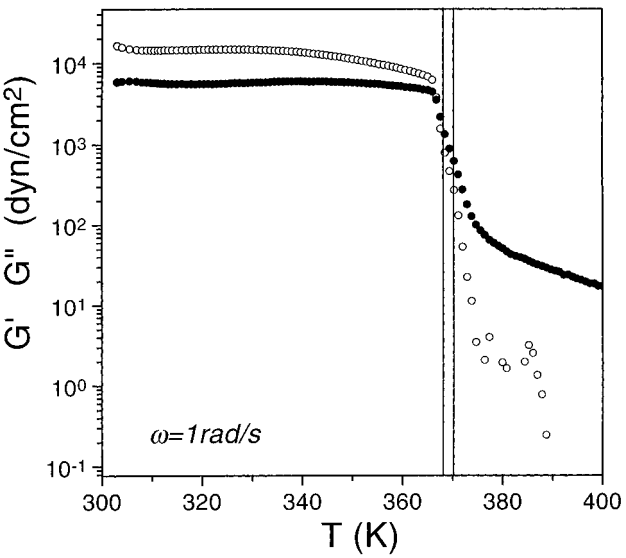

Figure 8. Isochronal measurements of the storage and loss moduli of the miktoarm SI_3-40/DOP at 1 rad/s with a heating rate of 2 K/min. The two vertical lines indicate the transition range.

dependencies of the order of $\omega^{1/3}$ to $\omega^{1/4}$. An $\omega^{1/4}$ dependence has been predicted[30] for a strongly segregated cylindrical mesophase. Essential in understanding such weak frequency dependencies is a polydomain structure below the T_{ODT}. The rheological behavior at low frequencies however is very complex due to the multiple length scales (i.e., domain, grain, single chain) existing in ordered block copolymers. The identification of the different length scales is a part of the ongoing work in our laboratory.

Fluctuations below the ODT. The existence of metastable states below the ODT was first discussed by Fredrickson and Binder.[31] They constructed a classical homogeneous nucleation theory for the ordering of lamellar phases in symmetric diblock copolymers from a supercooled metastable disordered melt. The free energy barrier for the creation of a spherical droplet of ordered material within the disordered melt was $\Delta F \sim \bar{N}^{-1/3}\delta^{-2}$, where $\bar{N}$ is the Ginzburg parameter, $\bar{N}^{-1/3}$ is the familiar fluctuation correction term and $\delta = (\chi - \chi_{ODT})/\chi_{ODT}$ is the dimensionless undercooling parameter.

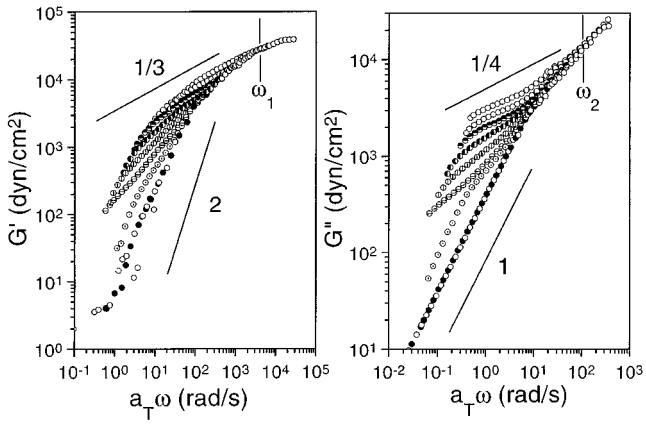

Figure 9. Reduced frequency plots for the storage and loss moduli of the miktoarm SI_3-45 diluted with DOP ($\varphi_P = 0.42$). The reference temperature was 364 K, and $T_{ODT} = 361$ K. Only data for some selected temperatures (K) are shown: (●) 362; (⊙) 360; (⊖) 357; (Φ) 354; (◐) 349, (◓) 344. The corresponding limiting slopes at low frequencies are also shown (2 and 1 for G' and G'', respectively).

The ordering time, $t_{1/2}$, was found to scale as $\exp(\Delta F/k_BT)$, and these predictions have been tested for symmetric diblock copolymers.[28,32] The case of anisotropic droplet shapes such as defected, anisotropic Wulff, and diffuse droplets was recently examined.[33] Furthermore, the kinetics of dissolution of hexagonal structures with the appearance of transient body-centered cubic structures as well as the kinetics of order-to-order transitions in weakly segregated microstructures has been studied.[34] The dissolution mechanism, however, occurs on a much faster time scale as compared to the ordering process,[35] which is controlled by the driving force δ; small values of δ result in very long incubation times. We have studied the ordering kinetics in various block copolymer architectures and found similar gross-features.[6,18,23] The ordering kinetics for shallow quenches proceed by nucleation and growth and the time-dependence of the volume fraction of ordered material can be described by the Avrami equation[36]

$$\phi(t) = 1 - \exp(-zt^n) \tag{10}$$

where z is the rate constant and n is the Avrami exponent, which is a combined function of the growth dimensionality and of the time-dependence of the nucleation and growth process. The effect of macromolecular architecture on the kinetics was to slow the characteristic ordering time, defined as $t_{1/2} = (\ln 2/z)^{1/n}$, for the case of star-shaped copolymers.[18]

The rheological kinetic experiments for the two miktoarm stars were conducted following temperature jumps from the high T disordered phase to different final temperatures below the ODT. The time evolution of G' and G'' was monitored immediately after the temperature jumps, and the results for the SI_3-45/DOP system are shown in Figure 10. Both moduli have an "S" shape with long-time plateau values which increase with decreasing temperature. This is also the expectation from the frequency dependent moduli at temperatures below the T_{ODT} and for frequencies below the characteristic frequencies $\omega_{1,2}$ (Figure 9). To extract the desired volume fraction ϕ of the ordered phase as it develops with time, we have used some very simple mechanical models[23] ("series" and "parallel") which provide limits for the mechanical response of a composite material as a function of the properties of the constituent phases (ordered and disordered). The re-

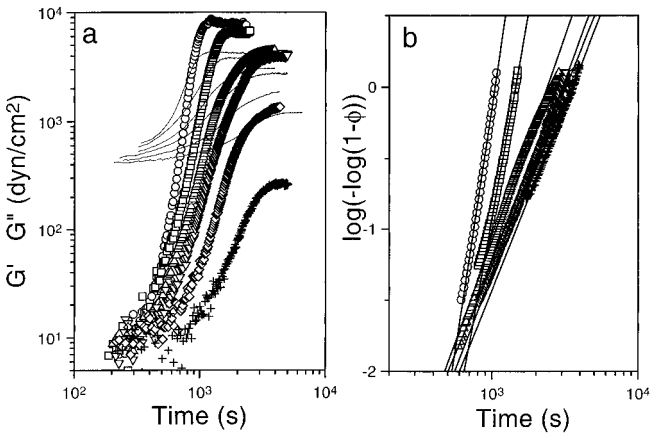

Figure 10. (a) Time evolution of G' (symbols) and G'' (lines) for the SI_3-45 miktoarm copolymer diluted with DOP (φ_P = 0.42), following a quench from the disordered phase (T_i = 367 K) to different final temperatures (K): (○) 355; (□) 356; (△) 357; (▽) 358; (◇) 359; (+) 360 K. (b) Avrami plots for the volume fraction of the ordered phase $\phi(t)$ for the same temperatures as in part a. Lines are fits to the Avrami equation.

Table 2. Parameters of the Avrami Equation for the SI_3-45/DOP Miktoarm Star Extracted from the Parallel Model (See Text)

T (K)	n	$\ln(t_{1/2}/s)$
360	2.6	7.7
359	2.5	7.6
358	2.8	7.57
357	2.9	7.35
356		~7.06
355		~6.5

sults for $\phi(t)$ are shown in Figure 10b and the solid lines are fits to the Avrami equation (eq 10). There is a steeper slope for the deeper quenches, similar to those for other diblock copolymers, and this probably indicates a different (faster) ordering mechanism at such temperatures. For shallow quenches the ordering mechanism proceeds via nucleation and growth with an Avrami exponent of about 3. The Avrami parameters are summarized in Table 2. The T-range where composition fluctuations dominate, and therefore metastable states can be observed, is very narrow and well within the predicted range of χN: $(\chi N_t)_c \leq \chi N_t \leq (\chi N_t)_c + 1$ by a recent density functional theory.[37] In conclusion, the ordering kinetics in the miktoarm stars, diluted with DOP, are reminiscent of other star-shaped copolymers and for shallow quenches belong to the Avrami class.

Conclusions

We have studied the process of microphase separation in the newly synthesized miktoarm star copolymers A_mB_n with $m \neq n$. The phase stability criteria have been explicitly calculated for AB_n with n up to 100. The theory predicts a maximum in the critical value of χN_t as a function of the number of arms n, for $n = 3$. This maximum arises from the delicate balance between the stretching free energies of the A and B blocks. These MFT predictions for the structure factor in the disordered phase and the spinodal have been tested experimentally for two AB_3 copolymers, and the results were found to be in qualitative agreement with theory. There is a discontinuous change of the structure factor at the T_{ODT}, signifying a first-order transition. Strong composition fluctuations exist in the system, giving rise to a curvature in the inverse peak intensity above the transition and to metastable states below. The latter are probed with rheology and reveal a nucleation and growth ordering mechanism for shallow quenches as with undiluted block copolymers.

Acknowledgment. G.F. acknowledges the support of the Alexander von Humboldt Foundation (FOKOOP), the Greek Secretariat for Research and Technology, and the Max-Planck Institute for Polymer Research for its hospitality.

References and Notes

(1) Gersappe, D.; Irvine, D.; Balazs, A. C.; Liu, Y.; Sokolov, J.; Rafailovich, M.; Schwarz, S.; Peiffer, D. G. *Science* **1994**, *265*, 1072.
(2) Shinozaki, A.; Jasnow, D.; Balazs, A. C. *Macromolecules* **1994**, *27*, 2496.
(3) Iatrou, H.; Hadjichristidis, N. *Macromolecules* **1992**, *25*, 4649.
(4) Iatrou, H.; Hadjichristidis, N. *Macromolecules* **1993**, *26*, 2479.
(5) Hadjichristidis, N.; Iatrou, H.; Behal, S. K.; Chludzinski, J. J.; Disko, M. M.; Garner, R. T.; Liang, K. S.; Lohse, D. J.; Milner, S. T. *Macromolecules* **1993**, *26*, 5812.
(6) Floudas, G.; Hadjichristidis, N.; Iatrou, H.; Pakula, T. Fischer, E. W. *Macromolecules* **1994**, *27*, 7735.
(7) Tselikas, Y.; Iatrou, H.; Hadjichristidis, N.; Liang, K. S.; Mohanty, K.; Lohse, D. J. *J. Chem. Phys.* **1996**, *105*, 2456.
(8) Milner, S. T. *Macromolecules* **1994**, *27*, 2333.
(9) Leibler, L. *Macromolecules* **1980**, *13*, 1602.
(10) Erukhimovich, I. Ya. *Vysokomol. Soedin* **1982**, *A24*, 1950 (translated in *Polym. Sci. USSR (Engl. Transl.)* **1982**, *24*, 2232).
(11) Olvera de la Cruz, M.; Sanchez, I. C. *Macromolecules* **1986**, *19*, 2501.
(12) Mayes, A. M.; Olvera de la Cruz, M. *J. Chem. Phys.* **1989**, *91*, 7228.
(13) Mayes, A. M.; Olvera de la Cruz, M. *J. Chem. Phys.* **1991**, *95*, 4670.
(14) Benoit, H.; Hadziioannou, G. *Macromolecules* **1986**, *21*, 1449.
(15) Dobrynin, A. V.; Erukhimovich, I. Ya. *Macromolecules* **1993**, *26*, 276.
(16) Strobl, G. R. *Acta Crystallogr.* **1970**, *A26*, 367.
(17) Fredrickson, G. H.; Helfand, E. *J. Chem. Phys.* **1987**, *87*, 697.
(18) Floudas, G.; Pispas, S.; Hadjichristidis, N.; Pakula, T.; Erukhimovich, I. *Macromolecules* **1996**, *29*, 4142.
(19) Floudas, G.; Hadjichristidis, N.; Stamm, M.; Likhtman, A. E.; Semenov, A. N. *J. Chem. Phys.* **1997**, *106*, 3318.
(20) Mori, K.; Tanaka, H.; Hasegawa, H.; Hashimoto, T. *Polymer* **1989**, *30*, 1389.
(21) Holzer, B.; Lehmann, A.; Stühn, B.; Kowalski, M. *Polymer* **1991**, *32*, 1935.
(22) Bates, F. S.; Rosedale, J. H.; Fredrickson, G. H. *J. Chem. Phys.* **1990**, *92*, 6255.
(23) Floudas, G.; Pakula, T.; Fischer, E. W.; Hadjichristidis, N.; Pispas, S. *Acta Polym.* **1994**, *45*, 176.
(24) Sakamoto, N.; Hashimoto, T. *Macromolecules* **1995**, *28*, 6825.
(25) Hashimoto, T.; Ijichi, Y.; Fetters, L. J. *J. Chem. Phys.* **1988**, *89*, 2463.
(26) Hashimoto, T.; Mori, K. *Macromolecules* **1990**, *23*, 2329.
(27) Mori, K.; Okawara, A.; Hashimoto, T. *J. Chem. Phys.* **1996**, *104*, 7765.
(28) Rosedale, J. H.; Bates, F. S. *Macromolecules* **1990**, *23*, 2329.
(29) Adams, L. J.; Graessley, W. W.; Register, R. A. *Macromolecules* **1994**, *27*, 6026.
(30) Rubinstein, M.; Obukhov, S. P. *Macromolecules* **1993**, *26*, 1740.
(31) Fredrickson, G. H.; Binder, K. *J. Chem. Phys.* **1989**, *91*, 7265.
(32) Floudas, G.; Vlassopoulos, D.; Pitsikalis, M.; Hadjichristidis, N.; Stamm, M. *J. Chem. Phys.* **1996**, *104*, 2083.
(33) Hohenberg, P. C.; Swift, J. B. *Phys. Rev. E* **1995**, *52*, 1828.
(34) Qi, S.; Wang, Z.-G. *Phys. Rev. Lett.* **1996**, *76*, 1679.
(35) Floudas, G.; Fytas, G.; Hadjichristidis, N.; Pitsikalis, M. *Macromolecules* **1995**, *28*, 2359.
(36) Avrami, M. J. *J. Chem. Phys.* **1939**, *7*, 1103; **1940**, *8*, 212; **1944**, *9*, 177.
(37) Muthukumar, M. *Macromolecules* **1993**, *26*, 5259.

MA961624L